Accepted Manuscript

On the volumetric properties of 2-hydroxy ethylammonium formate ionic liquid under high-pressures: Measurement and molecular dynamics

S.M. Hosseini, S. Aparicio, M.M. Alavianmehr, R. Khalifeh
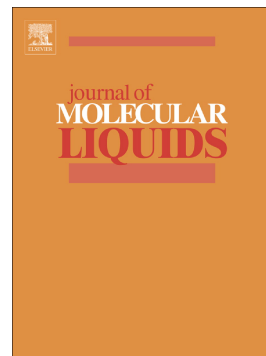
Please cite this article as: S.M. Hosseini, S. Aparicio, M.M. Alavianmehr, R. Khalifeh , On the volumetric properties of 2-hydroxy ethylammonium formate ionic liquid under high-pressures: Measurement and molecular dynamics. Molliq (2018), doi:10.1016/j.molliq.2018.06.074

This is a PDF file of an unedited manuscript that has been accepted for publication. As a service to our customers we are providing this early version of the manuscript. The manuscript will undergo copyediting, typesetting, and review of the resulting proof before it is published in its final form. Please note that during the production process errors may be discovered which could affect the content, and all legal disclaimers that apply to the journal pertain.

On the volumetric properties of 2-hydroxy ethylammonium formate ionic liquid under high-pressures: Measurement and molecular dynamics

S. M. Hosseini,[*a] S. Aparicio,[*b] M. M. Alavianmehr,[c] R. Khalifeh[c]

[a] Department of Chemistry, Faculty of Sciences, University of Hormozgan, Bandar Abbas 71961, Iran

[b] Department of Chemistry, University of Burgos, 09001 Burgos, Spain

[c] Department of Chemistry, Shiraz University of Technology, Shiraz 71555-313, Iran

[*]Corresponding authors: sm.hosseini@hormozgan.ac.ir (S.M. Hosseini) and sapar@ubu.es (S. Aparicio)

Abstract

This work aims to report not only the new measurement for densities of 2-hydroxy ethylammonium formate (2-HEAF) ionic liquid under high-pressures but also molecular dynamics considerations of nanoscopic characterization for physiochemical properties in the pressure range studied. High-pressure densities of 2-HEAF showed smooth trends with temperature and pressure variations. Measurements were carried out at temperatures T=(298.15 to 333.15) K and at pressures P=(0.1 to 40) MPa. The high-pressure densities of 2-HEAF have also been correlated by the use of Tait equation with AARD equal to 0.031% and the mechanical coefficients including the isothermal compressibility, isobaric expansivity and thermal pressure were estimated. Molecular dynamics simulations were carried out in the same pressure – temperature range as the experimental study. Force field was validated against experimental results and the microscopic structure was analyzed in terms of intermolecular interactions and their evolution with temperature and pressure.

1. Introduction

Detailed knowledge of the thermophysical properties of ionic liquids (ILs) are crucial due to their potential capabilities for both industrial and synthesis purposes. Among the thermophysical properties of ILs, their volumetric properties such as density should be known as it affects the mass transfer rates. It is also useful in piping, vessel designing and phase equilibrium calculations as well [1]. Knowing the density data as a function of temperature and pressure allows access to the mechanical coefficients such as the isothermal compressibility and isobaric expansivity and some thermal properties as well. The isothermal compressibility of ILs is relevant for the design of industrial fluids to be used in pumps or compressors [2]. As a third example, isobaric expansivity data of ILs are also required for their development as heat transfer fluids or for heat storage applications or, as recently suggested, for ionic liquid based liquid-in-glass thermometers [3]. Having the mechanical coefficients one can easily derive other thermodynamic properties such as the internal pressure being the change in internal energy of a liquid upon a small isothermal expansion.

Protic ionic liquids (PILs) are an interesting subset of ILs, with some distinguishing features when compared to aprotic ILs (AILs). The majority of PILs have non-negligible vapor pressures, but their beneficial properties for certain applications outweigh this potentially negative property [4]. The protic nature of PILs is a crucial feature in a number of applications, including biological applications [5], in organic synthesis [6-8], chromatography [9], as proton conducting electrolytes for polymer membrane fuel cells [10],self-assembly media [11-14], as catalysts [15].

2-hydroxy ethylammonium formate (2-HEAF), the IL investigated herein belongs to polar PILs and has been known for ease of synthesis and great solvation properties [16, 17] as well. It has also several unique properties; the highest electrical conductivity, lowest shear viscosity, and lowest melting point among the counterpart ILs make it highly useful for various industrial purposes. For example, its great solvation makes it promising option in the removal of CO_2 from industrial flue gas [18, 19]. Also, the IL under consideration is so polar that could be a promising media for some types of synthesis, in which polarity of solvent is of greatly importance such as that of high-thermally-stable ceramics. For example, polar ILs

1

have been used for the preparation of polyanion-type compounds as high performance cathode materials for Li-ion batteries [20].

Although several efforts have yet been reported on the measurement of density data of pure 2-HEA, all of which were limited to the ambient conditions or atmospheric pressure. An extensive literature survey of the previous efforts is available in the recent work of Hosseini et al. [21]. The atmospheric densities of 2-HEAF have yet been measured by the use of several apparatuses from non-digital ones like pycnometer [16] to those were based on the digital apparatus like vibrating-tube densimeter [17, 22-24].

This work is the continuation of our attempt to study of physiochemical property data of 2-HEAF. The aim is to report not only new measurements for density data of 2-HEAF but also molecular dynamic considerations, for which only one effort has been yet reported only under ambient condition [21]. The experimental results for the atmospheric densities (at 0.1 MPa) are going to be compared with the previously reported measurements [16, 24]. In addition the mechanical coefficients of 2-HEAF are calculated by the use of a Tait-type equation to derive the internal pressure of IL of interest. Theoretical studies using molecular dynamics (MD) simulations were carried out to obtain a microscopic view of 2-HEAF structuring and intermolecular forces, hydrogen bonding and their relationship with macroscopic behavior as a function of temperature and pressure. MD studies on the microscopic properties of ILs are very scarce in the literature. Aparicio et al. [25] studied tosylate and methylsulfate – based ionic liquids using MD simulations up to 60 MPa characterizing the increase in fluids' organization and changes in molecular arrangements with the increase of pressure. Zhao et al. [26] reported all-atoms MD simulations of 1-butyl-3-methylimidazolium hexafluorophosphate IL showing conformational changes in the cation upon pressure increase resulting in changes in density upon compression and large effects of pressure on ion mobility resulting in viscosity increase. Sharma et al. [27] showed the appearance of solid-like ionic arrangements for trihexyl(tetradecyl)phosphonium-based ILs with a large reorganization of molecular functionalities upon compression. Dhungana et al. [28] showed remarkable conformational changes upon compressions leading to the changes in physical properties and fluids' reorganization. In the particular case of PILs, Mariani et al. [29] reported for alkylammonium nitrate the development of mesoscopic disorder upon

2

compression with the loss of mesoscopic domain segregation. Therefore, MD simulations proposed in this work will contribute to the scarce available knowledge on the microscopic properties of PILs and their evolution with pressure increase with particular attention to the evolution of hydrogen bonding and its relationship with experimental properties.

2. Experimental procedure

2.1. Materials

All of the chemicals were analytical grade. Formic acid (Merck) and 2-aminoethanol (Merck) were distilled before use.

2.2. Preparation of the ionic liquid (2-hydroxy ethyl ammonium formate)

The details of the Preparation of the ionic liquid (2-hydroxy ethyl ammonium formate) have been previously discussed [21]. Also, in order to reduce water content of IL to at least magnitude, vacuum drying was performed for 24 h at 80° C was by the use of a vacuum oven. After that, the water contents of 2-HEAF were investigated using a coulometric Karl Fischer titrator DL 39 (Mettler Toledo) [22]. The results for the NMR spectra have also been reported earlier [21].

2.3. Density measurement apparatus

As mentioned above, the densities of 2-HEAF is going to be measured in the extended pressure ranging from 0.1 up to 40 MPa. To achieve this goal an experimental apparatus consisting of a digital density meter (Anton Paar DMA HPM) and pressure generator were employed. The digital density meter included a thermostatic bath, vibrating-tube densimeter and a barometer. The Vinci Technologies' digital density meter allows the fast measurement of densities via high pressure-high-temperature cell covering the range of fluid densities with a certified precision of $\pm 1 \times 10^{-4}$ g·cm^{-3}for the ambient pressures. However, that precision could be varied within 10^{-4} to 10^{-3} g·cm^{-3} depending on the range of the pressure ranging, in which the measurement is going to be carried out.

As Figure 1 depicts, the apparatus is provided with a thermostatic bath. Thermostating is made by a liquid jacket combined with an external thermostat bath for thermostating the

3

measuring cell. This apparatus allows access thermostating with temperature uncertainty of ± 0.1 K. The pressure is generated by a single cylinder pump (BTSP 500-5) from Vinci Technologies [30] and controlled with an Indumart Technology pressure gage with the accuracy of the order of 1.6%. The density meter is firstly calibrated at specific, constant pressure and temperature with two fluids of known density (nitrogen gas and liquid water as the representative for light and dense fluid herein), to derive the linear relationship between the natural frequency and fluid density at that pressure and temperature. The density can therefore be deduced from the measured frequency. The experimental uncertainties in the density were estimated to be better than $\pm 3.2 \times 10^{-4}$ g·cm^{-3}. The water content of the used samples was measured before (577ppm) and after experiments (864 ppm).

2.4. MD simulations

MD simulations were carried out using the MDynaMix v.5.2 program [31]. The force field parameterization for the studied ions was reported in a previous work [21]. Cubic simulation boxes containing 1000 ion pairs were used along the simulation and they were initially built using Packmol [32] program. Periodic boundary conditions were applied. Systems were simulated at 298, 313 and 333 K (selected as low, middle and high temperature for the experimental temperature range) and at 0.1, 5, 15, 25 and 40 MPa for each temperature (covering the experimental pressure range). Simulations were carried out in the NPT ensemble following a two steps procedure: i) equilibration runs (10 ns), with equilibration assured through the constancy of total potential energy, and followed by ii) production runs (50 ns). The control of pressure and temperature along the simulations was carried out with the Nose–Hoover method. the Tuckerman–Berne double time step method [33], with 1 and 0.1 fs for long and short time steps, was used for solving the equations of motion. Ewald method [34] was used for treating Coulombic interactions with a convergence parameter of 4.5 nm^{-1}, a cut-off radius of 1.5 nm for the real space part, and 9 terms for the reciprocal part. Lennard – Jones interactions were handled with 15 Å cutoff. The Lennard-Jones cross terms were calculated using Lorentz-Berthelot mixing rules.

4

3. Results and discussion

3.1. Density measurement under high-pressures

To show how are the results for atmospheric densities when compared with the literature data Figure 2 has been presented. Our results for density measurements at 0.1 MPa show some little absolute deviations (within 0.79-0.97%) from the work of Pinkert et al. [24] where the densities of 2-HEAF were measured by the use of Anton Paar DMA 602 H vibrating tube densimeter, but the deviations from the measurements of Ghatee et al. [16] (from pycnometric method)and Hosseini et al. [21] (from Anton PaarDSA-5000 vibrating-tube densimeter)are non-negligible (within 4.40-5.20%).

Figure 3 shows the experimental $P\rho T$ behavior of 2-HEAF at both isothermal (1a) and isobaric (1b) states. The solid lines are the best straight line passing thorough the experimental points. Measurements were carried out at temperatures T=(298.15 to 333.15) K and at pressures P=(0.1 to 40) MPa. High-pressure densities of 2-HEAF showed smooth trends with temperature and pressure variations. The numerical values of the measured densities of 2-HEAF have also been reported in Table 1.

3. 2. Tait equation correlation and mechanical coefficients

The Tait equation [35, 36] has been widely used in the literature for the description of density variation with the temperature and pressure. In the absence of the speed of sound data and the heat capacity the mechanical coefficients such as isothermal compressibility, κ_T, isobaric expansivity, α_P and thermal pressure coefficient, γ_v can be derived by the use of Tait equation. Generally, the calculation of the mechanical coefficients leads to useful information on the dependence of the volumetric properties on temperature and pressure. In this work, the $P\rho T$ data of 2-HEAF have been correlated using the Tait equation [36, 37] and then the above-mentioned mechanical coefficients were evaluated. Other thermodynamic properties such as the internal pressure, π_T can also be derived from this equation.

The Tait equation used in this work can be read as:

$$\rho(P,T) = \frac{\rho(P_0,T)}{\left[1 - C \ln\left(1 + \left(\frac{P}{B(T)}\right)\right)\right]} \tag{1}$$

$$\rho(P_0,T) = a_0 + a_1 T + a_2 T^2 \tag{2}$$

$$B(T) = b_0 + b_1 T + b_2 T^2 \tag{3}$$

Where, T is the absolute temperature in Kelvin and $\rho(P_0, T)$ is the density at ambient pressure P_0 and system temperature with units of $g \cdot cm^{-3}$. The $B(T)$ is temperature-dependent; C is a constant; and a_0-b_2 are fit parameters. The fit parameters of the Tait equation were determined by minimizing the following objective function and least-square method:

$$OF = \min \frac{100}{n} \sum_{i=1}^{n} \frac{|\rho(P,T)_i^{Exp.} - \rho(P,T)_i^{Corr.}|}{\rho(P,T)_i^{Exp.}} \tag{4}$$

where n represents the number of all density data points and $AARD$ is the average absolute relative deviation of the correlated results from the experimental data. The fit parameters of Tait equation together with the AARD (in %) of correlated high-pressure densities of 2-HEAF were reported in Table 2.

Figure S1 (see the Supplementary data file) depicts the deviations of experimental densities, ρ^{exp} of 2-HEAF from those calculated by the Tait equation (Eq. (1)), $\rho^{Calc.}$. It illustrates that the uncertainties of density fitting using the Tait equation have maximum value equal to$\pm0.085\%$. The coefficient of thermal expansion, α_P, being related to the variation of the density with temperature can be derived using the Tait equation as follow:

$$\alpha_P = -\frac{1}{\rho}\left(\frac{\partial \rho}{\partial T}\right)_P = -\frac{1}{\rho}\left\{ \begin{array}{l} \dfrac{(d\rho(P_0,T)/dT)}{1 - CLn\left(1 + \dfrac{P}{B(T)}\right)} - \dfrac{\rho(P_0,T)}{\left[1 - CLn\left(1 + \dfrac{P}{B(T)}\right)\right]^2} \\ \times \dfrac{CP(dB(T)/dT)}{B(T)^2\left(1 + \dfrac{P}{B(T)}\right)} \end{array} \right\} \tag{5}$$

The isothermal compressibility of the IL is calculated using the isothermal pressure derivative of the Tait equation as:

$$\kappa_T = \frac{1}{\rho}\left(\frac{\partial\rho}{\partial P}\right)_T = \frac{1}{\rho}\left\{\frac{\rho(P_0,T)}{\left[\frac{1}{C}-\ln\left(1+\frac{P}{B(T)}\right)\right]^2}\frac{C}{B\left(1+\frac{P}{B(T)}\right)}\right\} \tag{6}$$

The calculated values of κ_T are presented in Table 3. In the studied range of temperatures, (293.15 to 333.15) K, and pressures, (0.1 to 40) MPa, the isothermal compressibilities range in MPa^{-1} is, 3.4269×10^{-4} to 3.9405×10^{-4}. Also, Figure S2a (see the Supplementary data file) illustrates 2-HEAF becomes more compressible with increasing temperature and less compressible with increasing pressure. Generally, the isothermal compressibilities of ILs are similar to those of water and high-temperature molten salts and are less compressible than organic solvents due to the strong coulombic interactions between the ions [38, 39]

The results for isobaric expansivity values were reported in Table 4. In the studied range of temperatures, (293.15 to 333.15) K, and pressures, (0.1 to 40.0) MPa, isobaric expansivity range in K $^{-1}$is, 5.213 to 6.1994. Also, Figure S2b (see the Supplementary data file) illustrates 2-HEAF becomes less expansive with increasing temperature and pressure. Generally, isobaric expansivity coefficients, are typically between $(4-8)\times10^{-4}$ K^{-1} which is comparable with water and lower than that of organic solvents [39]. The literature survey of the previous efforts [40-42] reveals that the γ_υ values of ILs decrease with temperature and increase slightly with pressure. The results for γ_υ values of 2-HEAF reported in Table 5 and shown in Figure S2c (see the Supplementary data file), reveal that γ_υ increases slightly with pressure at most 0.12 MPa·K^{-1} but those values are not almost constant in the temperature range studied and vary with the temperature within ±0.3 MPa·K^{-1}.

The internal pressure, π_T values of the ILs are higher than those of organic solvents and water because of a higher electrostatic interactions in IL [42]. However, in the case of proptic ILs, the lower π_T values than classic molten salts is due to other types of molecular interactions in the protic IL, such as polarization and hydrogen bonding in addition to electrostatic interactions as seen purely in molten salts. Table 6 shows that the internal pressure decreases with increasing pressure for the temperatures between (298.15 and 328.15) K, and increases at 333 K because the resultant forces under low-pressure conditions are

attractive and as the pressure increases the repulsive forces become dominant at low temperatures for the IL. Table 6 also reveals that the π_T decreases with respect to temperature at fixed pressure for the IL just like what has previously been observed for normal liquids due to the fact that the increase in temperature only affects the coordination number, while the intermolecular distances within the liquid molecules remain unchanged [43]. The obtained temperature coefficient $\left(\frac{\partial \pi_T}{\partial T}\right)<0$ of 2-HEAF indicates that the IL is a type of associated or strongly associated liquid that is linked by hydrogen bonds. This observation is in accord with the previously reported theoretical studies for 2-HEAF [21], where the quantum chemical computations and molecular dynamics verified that two hydrogen bonds can be developed for a single cation-anion ion pair; the first one is the cation-anion hydrogen bonding and the second one is relevant to the self–association of cation-cation through hydrogen bonding between hydroxyl groups.

It would also be interesting to investigate the pressure dependence of isobaric heat capacity difference, ΔC_P of 2-HEAF between reference pressure (0.1 MPa herein) and a given pressure because heat capacity is most directly related to the structure of the liquid state [44]. Having the volumetric measurements one can easily get some useful information on the effect of pressure on the heat capacity difference of liquids between a reference pressure and a given pressure [45, 46].

The pressure dependence of isobaric heat capacity is described by the thermodynamic formula [40, 47]:

$$\left(\frac{\partial C_P}{\partial P}\right)_T = -T\left(\frac{\partial^2 V_m}{\partial T^2}\right)_P = -T\,\frac{M}{\rho}\left[\left(\frac{\partial \alpha_P}{\partial T}\right)_P + \alpha_P^2\right] \tag{7}$$

Where C_P is the isobaric heat capacity, P is the pressure, V_m is the molar volume, ρ is the molar density, T is the temperature, M is the molecular mass. In Eq. (7), α_P is that of thermal expansion coefficient and ρ is the liquid density both of which can be easily determined by the Tait. Integration over the above-mentioned equation leads to the following expression for the heat capacity difference from the reference state as [40]:

$$\Delta C_P(T, P) = -T \int_{P^*}^{P} \frac{M}{\rho}\left[\left(\frac{\partial \alpha_P}{\partial T}\right)_P + \alpha_P^2\right] dP \tag{8}$$

where P^* is the reference pressure ($P^* = 0.1$ MPa).

8

Figure S3a (see the Supplementary data file) shows the isothermal variation of isobaric heat capacity differences, ΔC_P between reference pressure and a given pressure. As Figure S3a (see the Supplementary data file) demonstrates the variation trend is increasing at 298.15 K, 303.15 K and 313 K isotherms over the whole pressure range studied (0.1-40 MPa). However, the isotherm of 333.155 K shows some maxima for ΔC_P at ~30 MPa. Also, at 298.15 K, 303.15 K and 313 K isotherms the ΔC_P values of 2-HEAF become non-negligible as the pressure increases. It has been confirmed that, the heat capacity of simple liquids is supposed to decrease with pressure, reach minimum and start increasing over the middle-temperature range. The minima are flattened and pushed to higher pressures over the higher-temperature range [47]. However, the isotherms of isobaric heat capacity of 2-HEAF against the pressure, do not exhibit minima which reveals that behavior is in accord with the self-associated liquids [47], for which their isobaric heat capacity variations with the pressure are strongly affected by the mechanism of the self-association [47]. Anyhow, the pressure and temperature ranges of the derived data are not large enough, to yield final conclusions on the pressure–temperature behavior of 2-HEAF and its hydrogen bond structure. A further increase of pressure would be helpful to investigate the behavior of isobaric heat capacities and to establish more in detail information on the character of its self-association.

Figure S3b (see the Supplementary data file) shows the variation of isobaric heat capacity differences, ΔC_P with the temperatures studied. On the first glance, the positive sign of ΔC_P reveals C_P of 2-HEAF is increasing against the pressure at a given temperature. The latter, the variation of ΔC_P with the temperature is slightly increasing and linear in series 0.1-10 MPa and 0.1-20 MPa. However, the trends described by series 0.1- 30 MPa and 0.1-40 MPa are quite different; the reasons for appearing those trends may be associated with some mathematical inconsistency of the Tait equation or a change in the inter-molecular potential.

3.3. Results and discussion on MD studies

MD studies on the high pressure behavior of ILs are scarce in the literature, and thus, the results reported in the following section allow a microscopic characterization of 2-HEAF, which is complementary to the experimental thermophysical results reported in previous sections. Experimental pressure-temperature-density results reported in this work allow a

9

validation of the force field used for MD simulations along this work. In a previous study [21] the considered forcefield was validated at atmospheric pressure as a function of temperature (298.15 to 323.15 K range) showing deviation with density data in the 0.30 to 1.50 %, with an underestimation of density and other properties such as viscosity or surface tension in comparison with experimental data, but with reasonable deviations [48, 49] which confirms the suitability of the force field for describing 2-HEAF properties. A comparison of MD predicted densities with experimental for three isotherms in the 0.1 to 40 MPa range is reported in Figure 4. It should be remarked that experimental density data reported in this work for high pressure conditions and those previously reported at atmospheric pressure [21] were obtained with different apparatus, and thus, they are slightly different. In the case of high pressure density data, results in Figure 4a show that MD overpredicts experimental data reported in this work but are close to those reported by Ghatee et al. [16] and Hosseini et al. [21] at atmospheric pressure. Deviations with experimental density data are in the 2.8 to 4.6 % range for the studied pressure – temperature range, decreasing with increasing temperature and with small changes with increasing pressure for each isotherm, Figure 4b. Regarding derived properties, a comparison between experimental and predicted isothermal compressibility is reported in Figure 4c showing reasonable agreement, i.e. in both cases isothermal compressibility increases with increasing temperature and decreases with increases pressure. Nevertheless, the decrease of isothermal compressibility with increasing pressure is larger from experimental results than from MD simulations, e.g. at 298.15 K the isothermal compressibility decreases 7.98 % on going from 0.1 to 40 MPa from experimental results whereas MD predicts a decrease of 1.60 % with analogous behavior for all the studied isotherms.

The microscopic structuring of 2-HEAF was initially analyzed by the radial distribution functions (RDFs) reported in Figure 5. It was previously reported [21] that 2-HEAF microstructuring is characterized by the development of anion-cation hydrogen bonding between the hydroxyl group of HEA cation and the oxygen atoms in formate anion, therefore RDFs involving these atomic sites are included in Figure 5 as a function of pressure. RDFs show that cation-anion (Figure 5a) and cation-cation (Figure 5b) hydrogen bonding is maintained in the whole pressure range (up to 40 MPa), as the first narrow and intense peaks

10

in Figure 5a and 5b show, whereas anion-anion interactions are remarkably less important discarding hydrogen bonding. Results in Figure 5 show very minor pressure effects on RDFs, i.e. the structure of the fluid from the viewpoint of intermolecular interactions remains almost constant upon compression. This RDFs behavior agrees with previous literature results for other types of ILs, Mariani et al. [29] showed almost null changes in structure factor for several protic ionic liquids on going from ambient pressure to 100 MPa, as also reported by Zhao et al. [26] for alkylimidazolium-based ionic liquids. Nevertheless, very subtle changes in RDFs upon compression may be inferred when comparisons with values at 0.1 MPa are reported, especially for those values corresponding to the first solvation shells (defined with distances up to the first minima in Figure 5). In the case of cation-anion interactions, Figures 6a to 6c, a decrease in the first RDF peak upon compression is inferred, with this effect increasing with increasing pressure, i.e. a slight disruption of the first solvation shell of anions around cation is produced when compressing disrupting anion-cation interactions. For cation-cation RDFs, Figures 6d to 6f and analogous effect is inferred to that for anion-cation ones, whereas in the case of anion-anion interactions, Figures 9g to 9i, RDFs are reinforced upon compression. There are also effects on the second solvation shells, especially for anion-cation interactions which are slightly reinforced upon compressions. It should be remarked that all these effects are minor but clear trends are inferred for the studied pressure range for all then interacting pairs which show minor but systematic rearrangements of solvation shells, especially for the first one, around each type of ion.

The effect of pressure on relevant torsion angles was also studied to infer if the cyclic mechanism of HEA-FOR interaction, hydrogen bonding, previously reported for atmospheric pressure conditions [21] was maintained upon compression. Results in Figure 7a for the torsion angle N-CA1-CA2-OA in HEA show the two relevant peaks at $\sim \pm 76^{\mathbf{o}}$ together with the $\sim \pm 56^{\mathbf{o}}$ for the CA1-CA2-OA-HA agrees with a non-linear arrangement of the hydroxyethyl chain in HEA because of cyclic hydrogen bonding with formate cation, which is maintained in the studied pressure range.

It may be expected that increasing pressure will modify dynamic properties of 2-HEAF, especially for ionic movement in the solvation spheres, which is quantified through the residence times reported in Figure 8 (calculated as explained in Ref. [21]). Low residence

11

times are obtained for all the considered solvation spheres, confirming the lability for the developed hydrogen bonds. Residence times decrease with increasing temperature, especially for HEA-FOR and HEA-HEA solvation shells, and increases with increasing pressure for all the shells. Nevertheless, the increase of residence times upon compression is very minor in the studied pressure range, and thus, confirming the minor effect of pressure on the structural (RDFs in Figures 5 and 6) and dynamic (Figure 8) properties of solvation shells. Nevertheless, the minor changes in microscopic dynamic properties is accompanied by non-negligible changes in macroscopic dynamic properties as reported in Figure 9 for self-diffusion coefficients (calculated from the slopes of mean square displacement, *msd*, and Einstein's equation, for fully diffusive regimes assured by log-log plots of *msd* vs simulation time with slopes close to unit) and dynamic viscosity (inferred from Green-Kubo equation). Self-diffusion coefficients decrease upon compression (~ 25 % on going from 0.1 to 40 MPa), with larger effects for lower temperatures, which agrees with the ~ 34 % increase of dynamic viscosity. Therefore, compression leads to a non-negligible decrease of molecular mobility in spite of very minor changes in structural and microscopic dynamics properties reported in Figures 5 to 8. Therefore, the microscopic roots of these changes in macroscopic physicochemical properties need to be analyzed. Despite the minor changes in structural properties of anion-cation interactions upon compression reported in Figures 5 and 6, changes in intermolecular interaction energies are obtained when pressure is increased, Figure 13. HEA-FOR interaction energies reported in Figure 10a show a non-linear increase (in absolute value) with increasing pressure, which is also inferred for the total intermolecular interaction energy, Figure 10b, which can be a factor decreasing molecular mobility and increasing viscosity in spite of maintaining similar structural arrangements upon compression. Nevertheless, the reinforcement of anion-cation interactions with increasing pressure is not a large effect, e.g. for HEA-FOR intermolecular interaction energy increases only a 2 % from 0.1 to 40 MPa at 298 K (similar effects for other interactions and temperatures, Figure 10a), which can not justify the large increase of macroscopic dynamic properties reported in Figure 9 or the increase in density reported in Figure 4. This is confirmed by the calculated hydrogen bonds per ion reported in Figure 11, which show a very minor increase with increase pressure. The hypothesis considered to justify the changes in macroscopic physicochemical properties

12

stands on the rearrangement of available empty space (holes) upon compression, which would lead to higher viscosity, lower molecular mobility and a slight increase of intermolecular interactions but maintaining the structural properties of solvation shells and mechanism of interionic interactions. For confirming this behavior, the distribution of cavities in 2-HEAF was calculated for the studied pressure range. The distribution of cavities was calculated by defining a grid o points distributed in the simulation cells and calculating the distances from each point to the limit of the closes atom, defined by its van der Waals radium, i.e. spherical cavities are defined. It should be remarked that cavities in the studied fluid can not be spherical and they may have complex geometries, but the consideration of spherical cavities is a suitable approach to analyze the distribution of empty space in 2-HEAF and the changes upon compression. Results in Figure 12 show the distribution of spherical cavities in 2-HEAF at 333 K a pressure up to 40 MPa. These results show the appearance of a complex cavities size distribution, with a strong distribution peak corresponding to cavities with roughly 0.13 Å radius and two additional peaks at with roughly 0.25 and 0.45 Å radii. The pressure effect on the 0.25 and 0.45 Å radii cavities can not be inferred (no changes for the studied range) but in the case of the peak corresponding to the most probable cavities size (0.13 Å) shows a minor but well defined peak toward smaller radii with increasing compression. This is confirmed in Figure 13a showing a non-linear decrease with pressure of the most probable spherical cavity size with increasing pressure, which is highly correlated with the increase of pressure, Figure 13b. Therefore, very subtle but systematic rearrangement of the available empty space upon compression is inferred, which combined with the slight increase in intermolecular interaction energies should be the two factors controlling the increase in density and decrease of molecular mobility with increasing pressure, but maintain the mechanism of anion-cation interactions in the studied pressure range.

4. Conclusions

This paper aimed to supplement the available experimental density data of 2-HEAF especially those not yet reported in the extended pressure ranging. The experimental $P\rho T$ data of 2-HEAF allowed access to both mechanical coefficients and some thermal properties.

In this study, the Tait equation has been employed to predict some behaviors appearing in thermal properties of the IL under consideration such as internal pressure and isobaric heat capacity difference from the reference pressure. In some cases the Tait equation was capable of predicting the associating character of the IL in accord with the preceding results obtained from the computational methods. However, some mathematical inconsistencies were found when the Tait equation was used to calculate the variation of isobaric heat capacity difference from the reference pressure with the temperature which might be due to a change in inter-molecular potential.

Comparison with the previously reported literature data on atmospheric density reveals some disagreements between the values reported by Refs. [16, 21] with those reported in this work and Ref. [24]. This is might be due to fact that the thermophysical property data of IL systems cannot be determined accurately regardless of the method used and water content as well. That is why, some significant discrepancies are appeared among the reported results up to now for 2-HEAF.

The reported molecular dynamics results in the studied temperature-pressure range showed very minor changes in interionic interactions upon compression, anion-cation interactions are slightly reinforced with increasing pressure but the structure of solvation shells and the extension of hydrogen bonding remains almost constant up to 40 MPa. A rearrangement of the available empty space with increasing pressure is inferred, decreasing cavities size, which combined with the reinforcement of interionic interactions should be the main reason of changes in macroscopic thermophysical properties. Nevertheless, it should be remarked that although the structure of the studied ionic liquid suffers minor and subtle microscopic changes with increasing pressure, they lead to non-negligible changes in macroscopic properties. Very high pressures would be required to produce remarkable changes in the microscopic structure of 2-HEAF confirming the stability of interionic interactions and arrangements for this ionic liquid in agreement with previous studies for other types of ionic liquid showing their suitability to be used up to high pressures without too large changes in their properties.

14

Literature cited

[1] D. Rabari, N. Patel, M. Joshipura, T. Banerjee, Densities of Six Commercial Ionic Liquids: Experiments and Prediction Using a Cohesion Based Cubic Equation of State, Journal of Chemical & Engineering Data, 59 (2014) 571-578.

[2] T. Predel, E. Schlücker, P. Wasserscheid, D. Gerhard, W. Arlt, Ionic liquids as operating fluids in high pressure applications, Chemical Engineering & Technology, 30 (2007) 1475-1480.

[3] H. Rodríguez, M. Williams, J.S. Wilkes, R.D. Rogers, Ionic liquids for liquid-in-glass thermometers, Green Chemistry, 10 (2008) 501-507.

[4] T.L. Greaves, A. Weerawardena, C. Fong, I. Krodkiewska, C.J. Drummond, Protic ionic liquids: solvents with tunable phase behavior and physicochemical properties, The Journal of Physical Chemistry B, 110 (2006) 22479-22487.

[5] J. Pernak, I. Goc, I. Mirska, Anti-microbial activities of protic ionic liquids with lactate anion, Green Chemistry, 6 (2004) 323-329.

[6] R.V. Hangarge, D.V. Jarikote, M.S. Shingare, Knoevenagel condensation reactions in an ionic liquid, Green Chemistry, 4 (2002) 266-268.

[7] K.K. Laali, V.J. Gettwert, Electrophilic nitration of aromatics in ionic liquid solvents, The Journal of organic chemistry, 66 (2001) 35-40.

[8] Y. Hu, J. Chen, Z.G. Le, Q.G. Zheng, Organic reactions in ionic liquids: ionic liquids ethylammonium nitrate promoted knoevenagel condensation of aromatic aldehydes with active methylene compounds, Synthetic communications, 35 (2005) 739-744.

[9] C.F. Poole, Chromatographic and spectroscopic methods for the determination of solvent properties of room temperature ionic liquids, Journal of chromatography A, 1037 (2004) 49-82.

15

[10] M.A. Susan, A. Noda, S. Mitsushima, M. Watanabe, Brønsted acid–base ionic liquids and their use as new materials for anhydrous proton conductors, Chemical Communications, DOI (2003) 938-939.

[11] W. Tamura-Lis, L. Lis, P. Quinn, Structures and mechanisms of lipid phase transitions in nonaqueous media. Dipalmitoylphosphatidylethanolamine in fused salt, Biophysical journal, 53 (1988) 489.

[12] J.C. Galvez-Ruiz, G. Holl, K. Karaghiosoff, T.M. Klapotke, K. Loehnwitz, P. Mayer, H. Noeth, K. Polborn, C.J. Rohbogner, M. Suter, Derivatives of 1, 5-Diamino-1 H-tetrazole: A New Family of Energetic Heterocyclic-Based Salts Inorganic Chemistry 2005, 44 (12), 4237−4253, Inorganic Chemistry, 44 (2005) 5192-5192.

[13] W. Tamura-Lis, L. Lis, P. Quinn, Thermodynamic characterization of phospholipids dispersed in ethylammonium nitrate (a fused salt), Journal of colloid and interface science, 150 (1992) 200-207.

[14] W. Tamura-Lis, L. Lis, P. Quinn, Structures and mechanisms of lipid phase transitions in nonaqueous media: dipalmitoylphosphatidylcholine in fused salt, Journal of Physical Chemistry, 91 (1987) 4625-4627.

[15] T. Jiang, H. Gao, B. Han, G. Zhao, Y. Chang, W. Wu, L. Gao, G. Yang, Ionic liquid catalyzed Henry reactions, Tetrahedron letters, 45 (2004) 2699-2701.

[16] M.H. Ghatee, M. Bahrami, N. Khanjari, H. Firouzabadi, Y. Ahmadi, A functionalized high-surface-energy ammonium-based ionic liquid: experimental measurement of viscosity, density, and surface tension of (2-hydroxyethyl) ammonium formate, Journal of Chemical & Engineering Data, 57 (2012) 2095-2101.

[17] N. Bicak, A new ionic liquid: 2-hydroxy ethylammonium formate, Journal of Molecular Liquids, 116 (2005) 15-18.

[18] M. Ramdin, T.W. de Loos, T.J. Vlugt, State-of-the-art of CO2 capture with ionic liquids, Industrial & Engineering Chemistry Research, 51 (2012) 8149-8177.

[19] M. Hasib-ur-Rahman, M. Siaj, F. Larachi, Ionic liquids for CO 2 capture—development and progress, Chemical Engineering and Processing: Process Intensification, 49 (2010) 313-322.

16

[20] Z. Gong, Y. Yang, Recent advances in the research of polyanion-type cathode materials for Li-ion batteries, Energy & Environmental Science, 4 (2011) 3223-3242.

[21] S.M. Hosseini, M.M. Alavianmehr, A. Gutiérrez, R. Khalifeh, J. Moghadasi, S. Aparicio, On the properties and structure of 2-hydroxyethylammonium formate ionic liquid, Journal of Molecular Liquids, 249 (2018) 233-244.

[22] X.L. Yuan, S.J. Zhang, X.M. Lu, Hydroxyl ammonium ionic liquids: synthesis, properties, and solubility of SO2, Journal of Chemical & Engineering Data, 52 (2007) 596-599.

[23] K. Kurnia, C. Wilfred, T. Murugesan, Thermophysical properties of hydroxyl ammonium ionic liquids, The Journal of Chemical Thermodynamics, 41 (2009) 517-521.

[24] A. Pinkert, K.L. Ang, K.N. Marsh, S. Pang, Density, viscosity and electrical conductivity of protic alkanolammonium ionic liquids, Physical Chemistry Chemical Physics, 13 (2011) 5136-5143.

[25] S. Aparicio, R. Alcalde, B. Garcia, J.M. Leal, High-pressure study of the methylsulfate and tosylate imidazolium ionic liquids, The Journal of Physical Chemistry B, 113 (2009) 5593-5606.

[26] Y. Zhao, X. Liu, X. Lu, S. Zhang, J. Wang, H. Wang, G. Gurau, R.D. Rogers, L. Su, H. Li, The behavior of ionic liquids under high pressure: A molecular dynamics simulation, The Journal of Physical Chemistry B, 116 (2012) 10876-10884.

[27] S. Sharma, A. Gupta, D. Dhabal, H.K. Kashyap, Pressure-dependent morphology of trihexyl (tetradecyl) phosphonium ionic liquids: A molecular dynamics study, The Journal of Chemical Physics, 145 (2016) 134506.

[28] K.B. Dhungana, C.J. Margulis, Comparison of the Structural Response to Pressure of Ionic Liquids with Ether and Alkyl Functionalities, The Journal of Physical Chemistry B, 121 (2017) 6890-6897.

[29] A. Mariani, R. Caminiti, M. Campetella, L. Gontrani, Pressure-induced mesoscopic disorder in protic ionic liquids: first computational study, Physical Chemistry Chemical Physics, 18 (2016) 2297-2302.

[30] High pressure syringe pump, , Vinci Technologies SA, http://www.vinci-technologies.com.

[31] A.P. Lyubartsev, A. Laaksonen, M. DynaMix–a scalable portable parallel MD simulation package for arbitrary molecular mixtures, Computer Physics Communications, 128 (2000) 565-589.

[32] L. Martínez, R. Andrade, E.G. Birgin, J.M. Martínez, PACKMOL: a package for building initial configurations for molecular dynamics simulations, Journal of Computational Chemistry, 30 (2009) 2157-2164.

[33] M. Tuckerman, B.J. Berne, G.J. Martyna, Reversible multiple time scale molecular dynamics, The Journal of Chemical Physics, 97 (1992) 1990-2001.

[34] U. Essmann, L. Perera, M.L. Berkowitz, T. Darden, H. Lee, L.G. Pedersen, A smooth particle mesh Ewald method, The Journal of Chemical Physics, 103 (1995) 8577-8593.

[35] G. Tammann, The dependence of the volume of solutions on pressure, Z. Phys. Chem. Stoechiom. Verwandtschafts, 17 (1895) 620-636.

[36] J. Dymond, R. Malhotra, The Tait equation: 100 years on, International journal of thermophysics, 9 (1988) 941-951.

[37] J.H. Dymond, R. Malhotra, The Tait equation: 100 years onInt. J. Thermophys. 9 (1988) 941-951.

[38] E. Lemmon, M. McLinden, D. Friend, Thermophysical Properties of Fluid Systems in NIST Chemistry WebBook, NIST Standard Reference Database Number 69, Eds. Linstrom, PJ and Mallard, WG, National Institute of Standards and Technology, Gaithersburg MD, 20899, webbook. nist. gov (accessed October 28, 2012), 2011.

[39] Z. Gu, J.F. Brennecke, Volume expansivities and isothermal compressibilities of imidazolium and pyridinium-based ionic liquids, Journal of Chemical & Engineering Data, 47 (2002) 339-345.

[40] R.L. Gardas, M.G. Freire, P.J. Carvalho, I.M. Marrucho, I.M. Fonseca, A.G. Ferreira, J.A. Coutinho, High-pressure densities and derived thermodynamic properties of imidazolium-based ionic liquids, Journal of Chemical & Engineering Data, 52 (2007) 80-88.

[41] L.I. Tomé, P.J. Carvalho, M.G. Freire, I.M. Marrucho, I.M. Fonseca, A.G. Ferreira, J.A. Coutinho, R.L. Gardas, Measurements and correlation of high-pressure densities of imidazolium-based ionic liquids, Journal of Chemical & Engineering Data, 53 (2008) 1914-1921.

18

[42] J. Safarov, I. Kul, W.A. El-Awady, A. Shahverdiyev, E. Hassel, Thermodynamic properties of 1-butyl-3-methylpyridinium tetrafluoroborate, The Journal of Chemical Thermodynamics, 43 (2011) 1315-1322.

[43] M. Fedorov, V. Stahulenok, Internal pressure and its application for the analysis of the structure of aqueous electrolyte solutions at high temperatures and pressures, Journal of Structural Chemistry, 22 (1981) 140-142.

[44] S.L. Randzio, Dynamic calorimetry in high-pressure, high-temperature thermodynamics of liquids, Thermochimica acta, 121 (1987) 463-471.

[45] P. Bridgman, W. Bridgman, Collected Experimental Papers Harvard University Press, Cambridge (Mass.) VII, papers, 173 (1964) 4071.

[46] P. Bridgman, The Physics of High Pressure (Bell, London), Google Scholar, DOI (1958) 386.

[47] E. Wilhelm, T. Letcher, Heat capacities: liquids, solutions and vapours, Royal Society of Chemistry2010.

[48] S.N. Butler, F. Müller- Plathe, A Molecular dynamics study of viscosity in ionic liquids directed by quantitative structure–property relationships, ChemPhysChem, 13 (2012) 1791-1801.

[49] J. Ma, Z. Zhang, Y. Xiang, F. Cao, H. Sun, On the prediction of transport properties of ionic liquid using 1-n-butylmethylpyridinium tetrafluoroborate as an example, Molecular Simulation, 43 (2017) 1502-1512.

Table 1   Results for the measurement of density, ρ(g·cm^{-3}) of 2-HEAF over the pressure ranging from 0.1 MPa up to 40 MPa and several isotherms.

	ρ/ g·cm^{-3} at T/K							
P/MPa	298.15	303.15	308.15	313.15	318.15	323.15	328.15	333.15
0.1	1.1510	1.1478	1.1446	1.1411	1.1368	1.1343	1.1318	1.1281
5	1.153	1.1498	1.1463	1.1429	1.1394	1.1365	1.133	1.1299
10	1.1551	1.1519	1.1487	1.1451	1.1416	1.1386	1.1357	1.1319
15	1.1572	1.1541	1.1508	1.1473	1.1437	1.1407	1.1377	1.1339
20	1.1596	1.1563	1.1531	1.1495	1.1459	1.143	1.1400	1.1363
25	1.1618	1.1585	1.1552	1.1517	1.1481	1.1451	1.1421	1.1386
30	1.164	1.1607	1.1575	1.154	1.1504	1.1474	1.1442	1.1406
35	1.166	1.1629	1.1597	1.1562	1.1527	1.1496	1.1464	1.1427
40	1.1680	1.1650	1.1620	1.1587	1.1551	1.1520	1.1488	1.1454

[a]$\Delta\rho= \pm3.2\times10^{-4}$ g·cm^{-3}

[a] Uncertainties of the measured densities

Table 2   The fit parameters of the Tait equation along with the average absolute relative deviations of the fitting (AARD in %) used to smooth the experimental densities of 2-HEAF as a function of pressure (up to 40 MPa) and temperature (from 298 to 333 K).

C	a_0 g·cm^{-3}	a_1 g·cm^{-3}·K^{-1}	$a_2 \times 10^6$ g·cm^{-3}·K^2	$b_0 \times 10^{-4}$ MPa	b_1 MPa·K^{-1}	$b_2 \times 10^2$ MPa·K^{-2}	AARD (in %)
0.451	1.5147	-1.513	1.6905	1.2512	-68.762	10.378	0.031

$^a \Delta\rho = \pm 9 \times 10^{-4}$ g·cm^{-3}

[a] Uncertainty of calculated densities from the Tait equation

ACCEPTED MANUSCRIPT

21

Table 3 Results for the isothermal compressibility, κ_T of 2-HEAF calculated by the use of the Tait equation.

	$\kappa_T \times 10^4$ /MPa^{-1} at T/K							
P/MPa	298.15	303.15	308.15	313.15	318.15	323.15	328.15	333.15
0.1	3.7241	3.7697	3.8108	3.8476	.8787	3.9049	3.9255	3.9405
5	3.6846	3.7292	3.7694	3.8054	3.8358	3.8615	3.8816	3.8962
10	3.6452	3.6888	3.7282	3.7634	3.7931	3.8182	3.8379	3.8522
15	3.6067	3.6494	3.688	3.7224	3.7515	3.776	3.7953	3.8093
20	3.5691	3.6109	3.6487	3.6824	3.7108	3.7348	3.7537	3.7674
25	3.5323	3.5733	3.6103	3.6433	3.6711	3.6946	3.713	3.7264
30	3.4964	3.5365	3.5727	3.6051	3.6323	3.6554	3.6734	3.6865
35	3.4613	3.5006	3.5361	3.5677	3.5945	3.617	3.6346	3.6475
40	3.4269	3.4654	3.5002	3.5312	3.5574	3.5795	3.5968	3.6094

[a]$\Delta\kappa_T = \pm(0.151\times10^{-4})$ MPa^{-1}

[a] Uncertainty of calculated isothermal compressibilities from the Tait equation

Table 4   Results for the thermal expansivity coefficient, α_P of 2-HEAF calculated by the use of the Tait equation.

	$\alpha_P \times 10^4 /K^{-1}$ at T/K							
P/MPa	298.15	303.15	308.15	313.15	318.15	323.15	328.15	333.15
0.1	6.1994	6.0708	5.941	5.8086	5.6776	5.5436	5.4096	5.2738
5	6.1908	6.0623	5.9325	5.8002	5.6693	5.5355	5.4015	5.266
10	6.1822	6.0537	5.9239	5.7917	5.661	5.5272	5.3935	5.258
15	6.1737	6.0452	5.9155	5.7834	5.6527	5.5191	5.3855	5.2503
20	6.1653	6.0368	5.9072	5.7752	5.6446	5.5112	5.3777	5.2426
25	6.157	6.0286	5.8991	5.7671	5.6367	5.5033	5.37	5.235
30	6.1488	6.0205	5.891	5.7591	5.6288	5.4956	5.3624	5.2276
35	6.1408	6.0125	5.8831	5.7513	5.6211	5.4879	5.3549	5.2202
40	6.1328	6.0046	5.8752	5.7435	5.6134	5.4804	5.3475	5.213
[a]$\Delta\alpha_P = \pm(0.484\times10^{-4})$ K^{-1}								

[a] Uncertainty of calculated thermal expansivities from the Tait equation

Table 5   Results for the thermal pressure coefficient, γ_v of 2-HEAF calculated by the use of the Tait equation.

	γ_v /MPa·K^{-1} at T/K							
P/MPa	298.15	303.15	308.15	313.15	318.15	323.15	328.15	333.15
0.1	1.6647	1.6104	1.559	1.5097	1.4638	1.4196	1.3781	1.3384
5	1.6802	1.6256	1.5738	1.5242	1.478	1.4335	1.3916	1.3515
10	1.696	1.6411	1.5889	1.539	1.4924	1.4476	1.4053	1.3649
15	1.7117	1.6565	1.604	1.5537	1.5068	1.4616	1.419	1.3783
20	1.7274	1.6718	1.619	1.5683	1.5211	1.4756	1.4326	1.3916
25	1.743	1.6871	1.634	1.583	1.5354	1.4895	1.4462	1.4048
30	1.7586	1.7024	1.6489	1.5975	1.5496	1.5034	1.4598	1.418
35	1.7741	1.7176	1.6637	1.612	1.5638	1.5173	1.4733	1.4312
40	1.7896	1.7327	1.6785	1.6265	1.5779	1.5311	1.4867	1.4443

[a] $\Delta\gamma_v = \pm 0.160$ MPa·K^{-1}

[a] Uncertainty of calculated thermal pressure coefficients from the Tait equation

24

Table 6   Results for the internal pressure, π_T of 2-HEAF calculated by the use of the Tait equation.

	π_T /MPa at T/K							
P/MPa	298.15	303.15	308.15	313.15	318.15	323.15	328.15	333.15
0.1	536.18	517.85	501.49	486.97	474.68	464.16	455.61	448.86
5	527.81	510.34	494.97	481.59	470.54	461.38	454.28	449.08
10	519.28	502.68	488.32	476.1	466.3	458.54	452.92	449.29
15	510.73	495.01	481.66	470.6	462.06	455.69	451.56	449.51
20	502.19	487.34	475	465.09	457.82	452.85	450.2	449.71
25	493.64	479.66	468.34	459.59	453.57	449.99	448.83	449.92
30	485.09	471.99	461.67	454.08	449.32	447.14	447.46	450.12
35	476.54	464.3	455	448.56	445.07	444.28	446.09	450.32
40	467.98	456.62	448.33	443.04	440.81	441.42	444.71	450.51
[a]$\Delta\pi_T = \pm 50.66$ MPa								

[a] Uncertainty of calculated internal pressures from the Tait equation

Figure captions

Figure 1   The densitometer setup used in this work.

Figure 2   Experimental atmospheric density, ρ obtained in this work compared with those from Pinkert et al. [24], Ghatee et al. [16] and Hosseini et al. [21].

Figure 3   The experimental $P\rho T$ behavior of 2-HEAF at both isothermal (a-lot) and isobaric (b-plot) states. The solid lines are the best straight line passing thorough the experimental points

Figure 4   Comparison of experimental (EXP) and predicted (molecular dynamics, MD) for the reported isortherms of 2-HEAF. ρ and κ_T stand for density and isothermal compressibility, respectively.

Figure 5   Radial distribution functions, $g(r)$, for the reported atomic pairs at 333 K and the selected pressures for 2-HEAF. Values obtained from molecular dynamics simulations.

Figure 6   Differences between the radial distribution function at 0.1 MPa, $g(r)_{0.1\ MPa}$, and those at the reported pressures, $g(r)_P$, at the selected temperatures for the reported atomic pairs in 2-HEAF. Values obtained from molecular dynamics simulations.

Figure 7   Distribution of torsion angles, φ, from molecular dynamics simulations of 2-HEAF at 333 K and the reported pressures. Atom labelling as in   Figure 8.

Figure 8   Residence time, t_{res}, or ions around (ar) other ions from molecular dynamics simulations of 2-HEAF at 333 K and the reported pressures. Numbers in the plot indicate the slope of linear fits (in ps / MPa^{-1} units). X ar Y (where X and Y stand for 2-HEA or FOR) indicate residence time of X in the first solvation sphere around Y, with the solvation sphere defined by the first minima of the corresponding radial distribution functions.

Figure 9   (a) Self-diffusion coefficients, D, and (b) dynamic viscosity, η, for the reported temperatures and pressures from molecular dynamics simulations of 2-HEAF. Number in the plot indicate the percentage difference of the corresponding property between 40 and 0.1 MPa (+, increase and -, decrease).

Figure 10   Intermolecular interaction energy, E_{inter} (sum of Lennard-Jones and coulombic contributions), for (a) HEA-FOR interactions and (b) total (sum of HEA-FOR, HEA-HEA and FOR-FOR contributions) from molecular dynamics simulations of 2-HEAF at the reported temperatures and pressures.

Figure 11   Average number of hydrogen bonds per ion pair, N_H, between OA(HA), as donor, and OF(HF) as acceptor, with 3.5 Å and 60° as donor-acceptor distance and angle as hydrogen bonding criteria from molecular dynamics simulations of 2-HEAF at the 333 K and the reported pressures.

Figure 12   Probability distribution plots of spherical cavities with radius, R, in 2-HEAF at 333 K and the reported pressures. Values obtained from molecular dynamics simulations. The yellow arrow indicates increasing pressure.

Figure 13   Relationship between the maximum radius of spherical cavities for the stronger probability distribution peaks (first peak in Figure 12), R_{max}, and (a) pressure or (b) density from molecular dynamics simulations at 333 K.

27
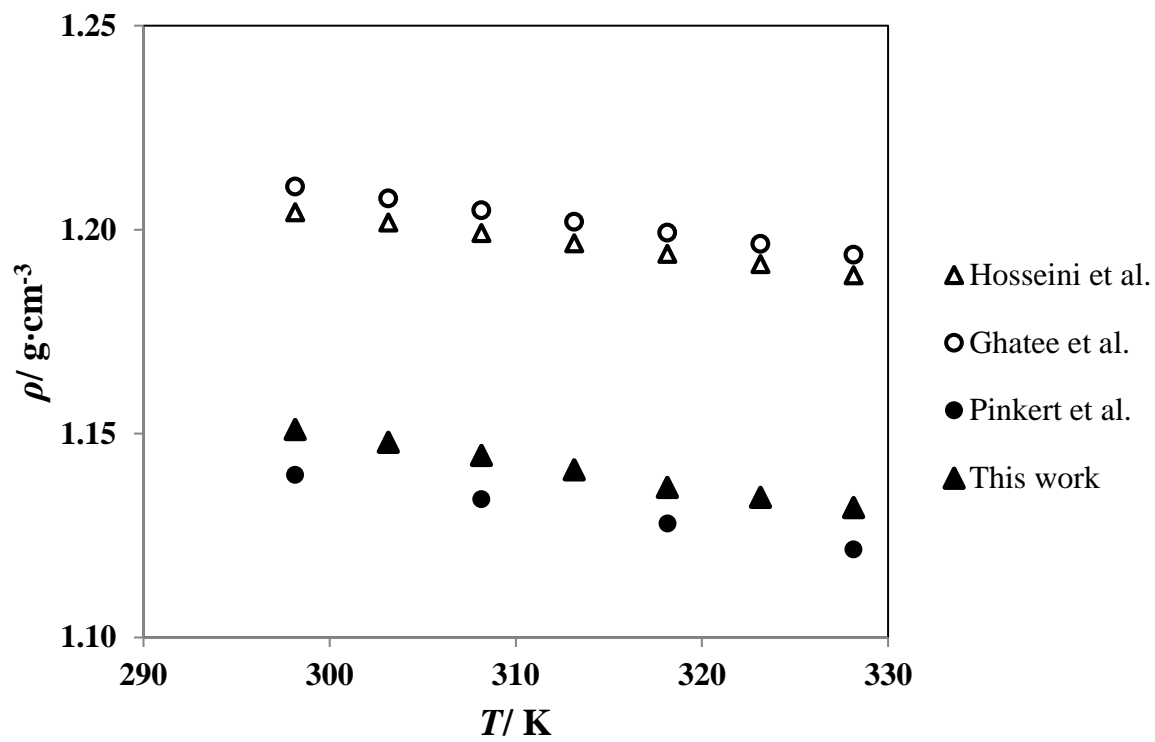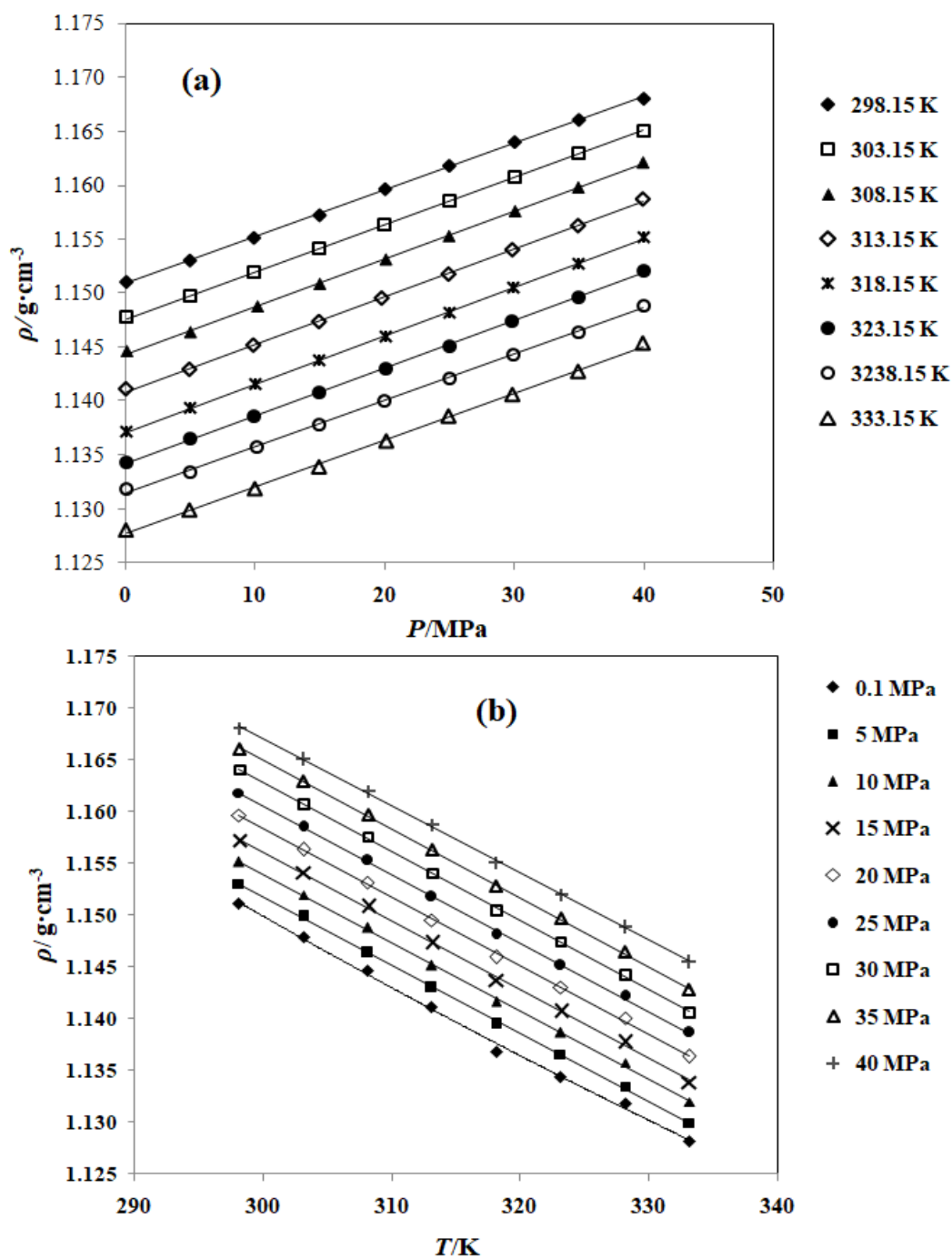
Figure 1

Figure 2

Figure 3

Figure 4

Figure 5

32

Figure 6

33
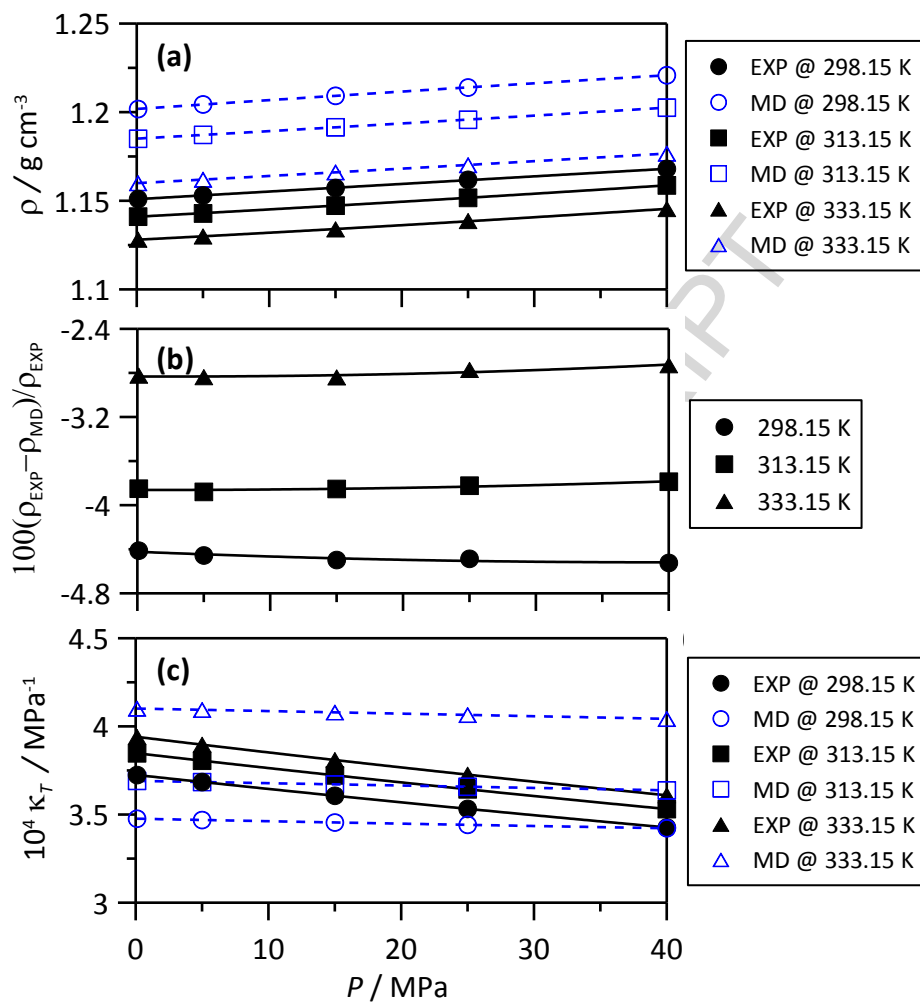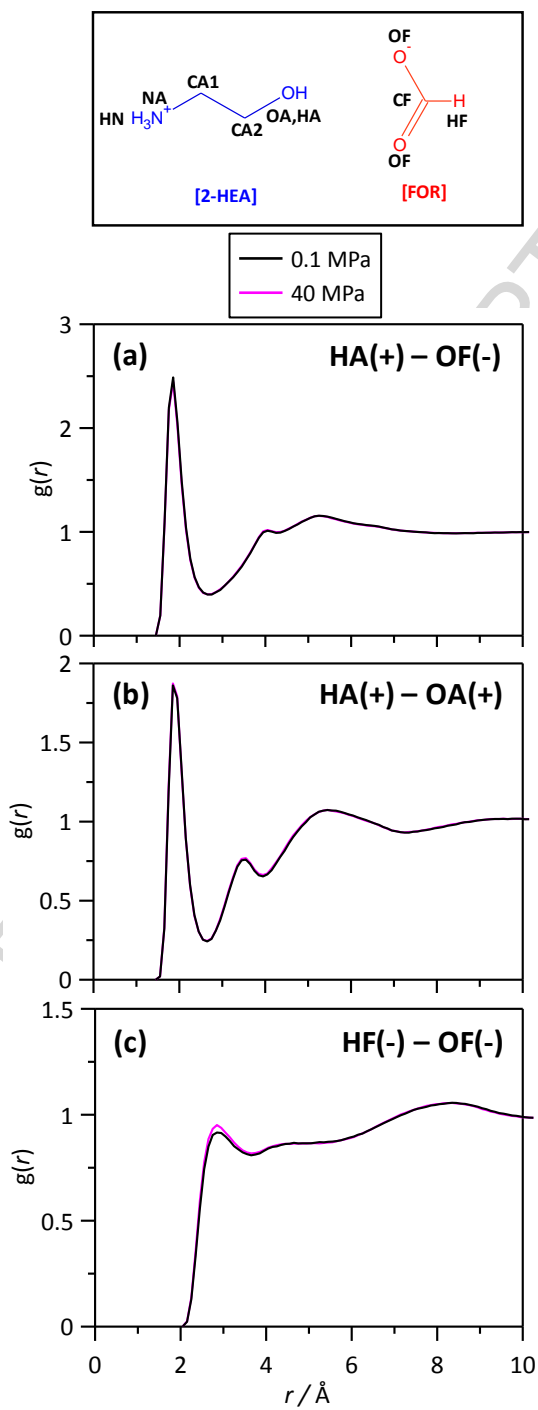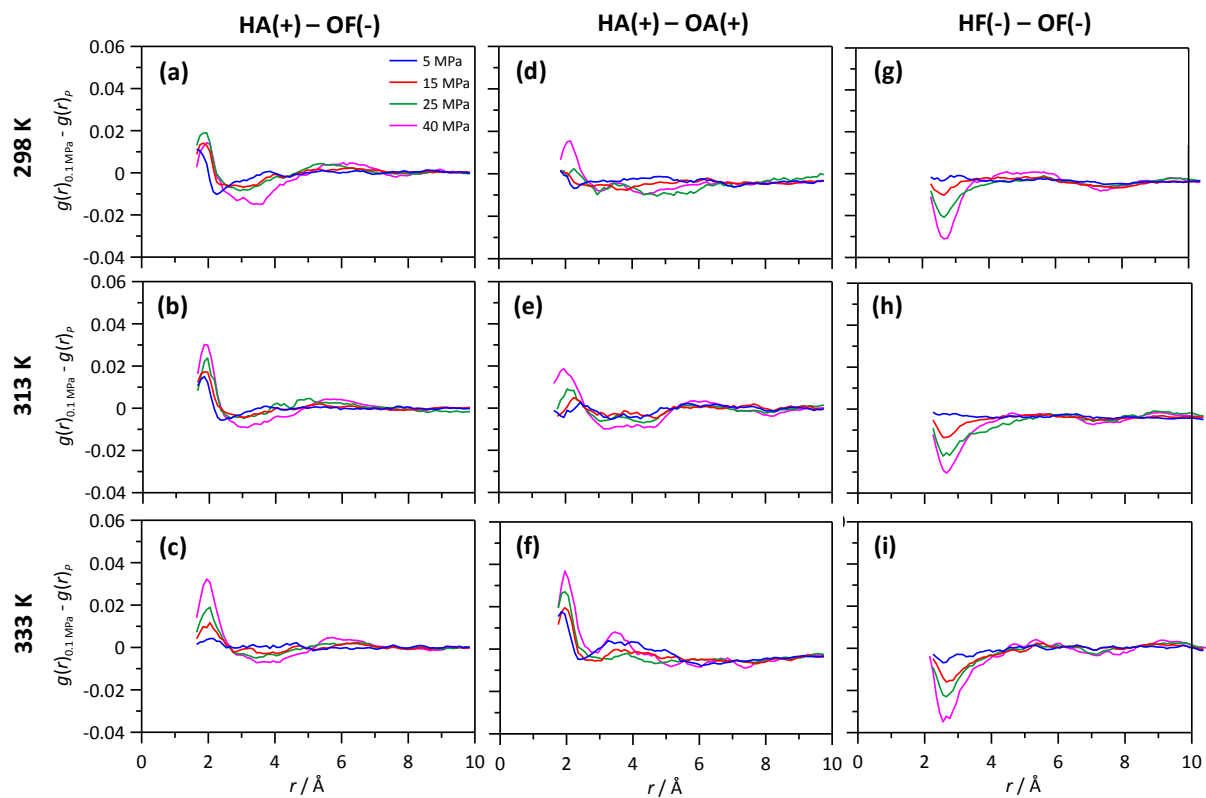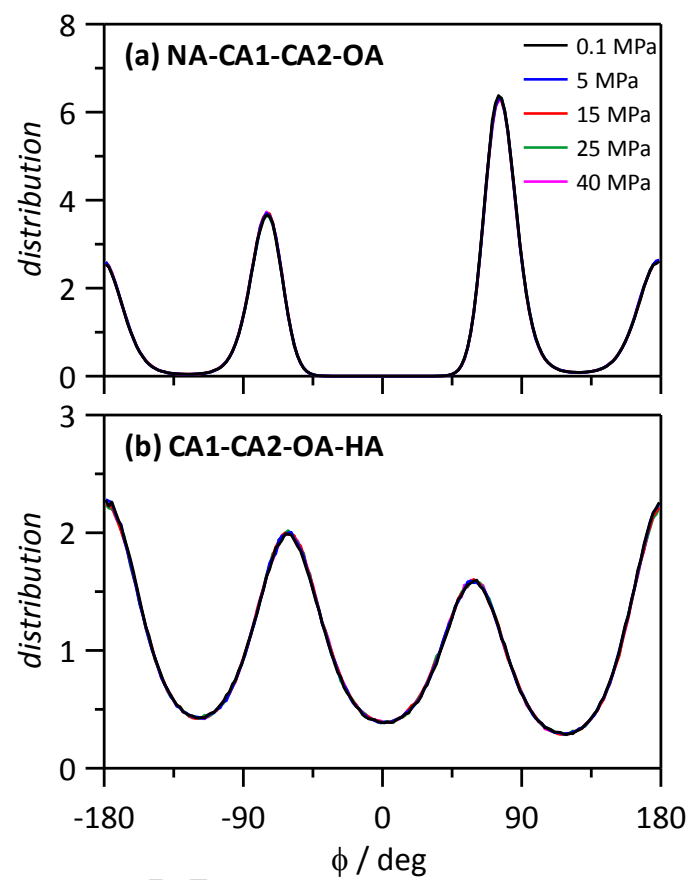
Figure 7

Figure 8

Figure 9

36
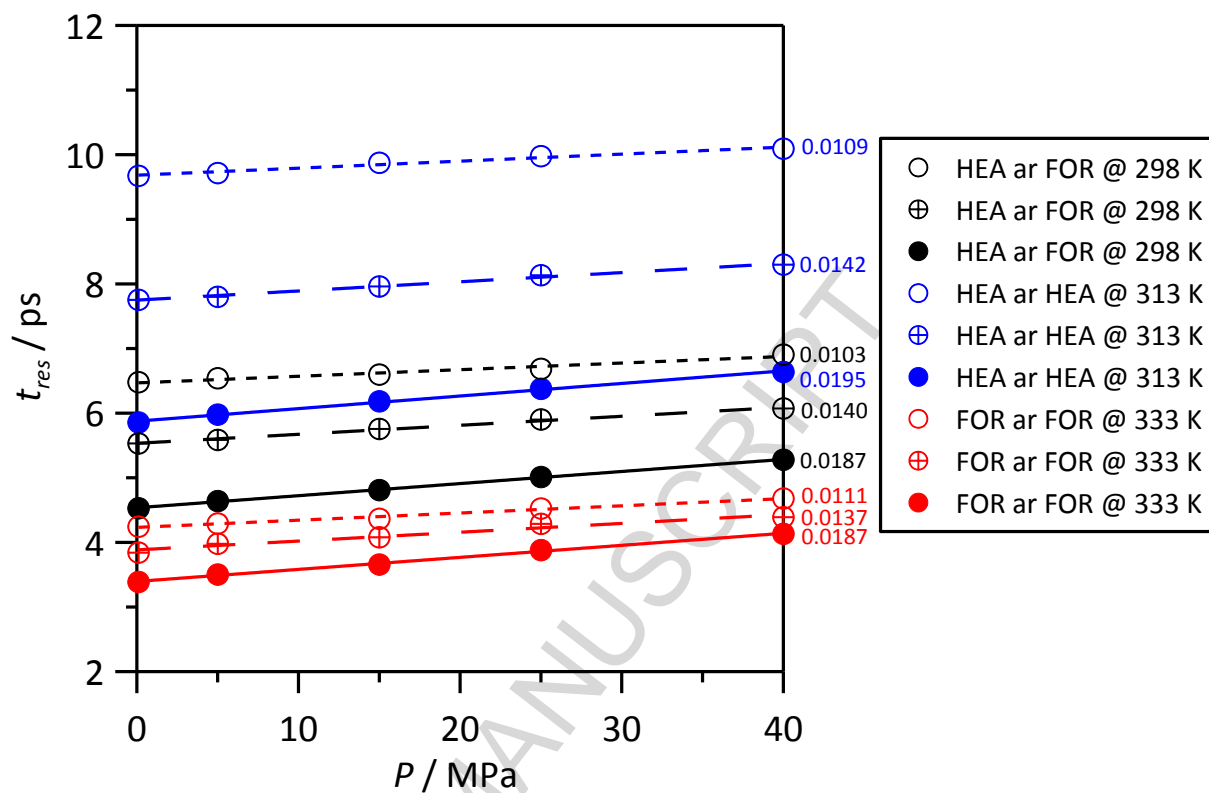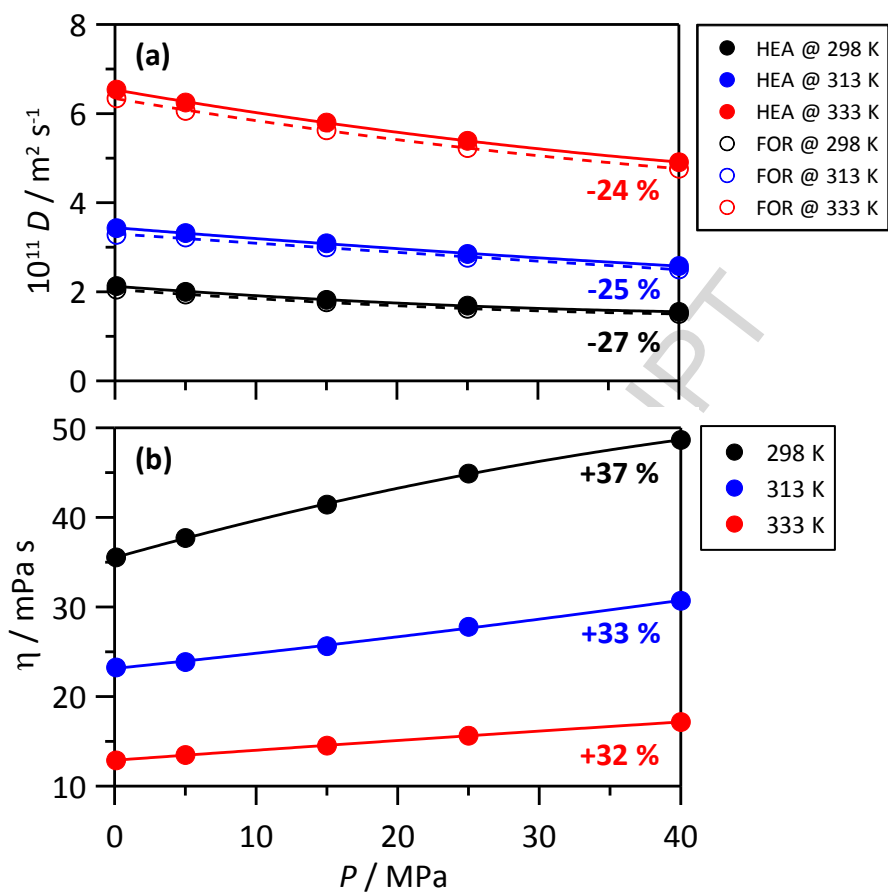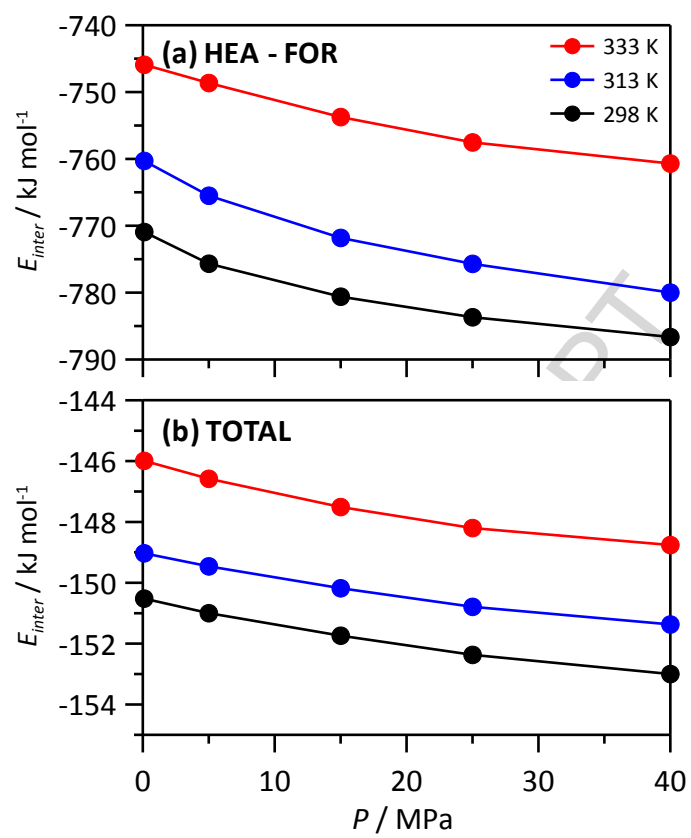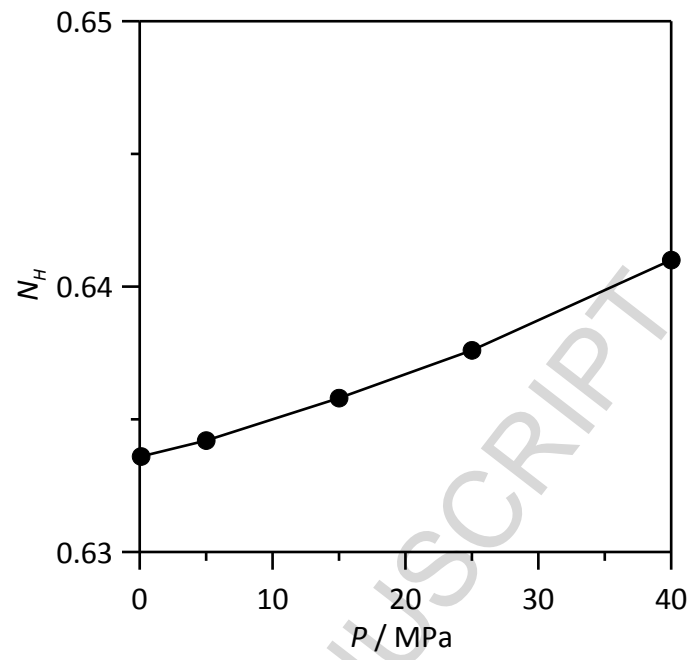
Figure 10

Figure 11
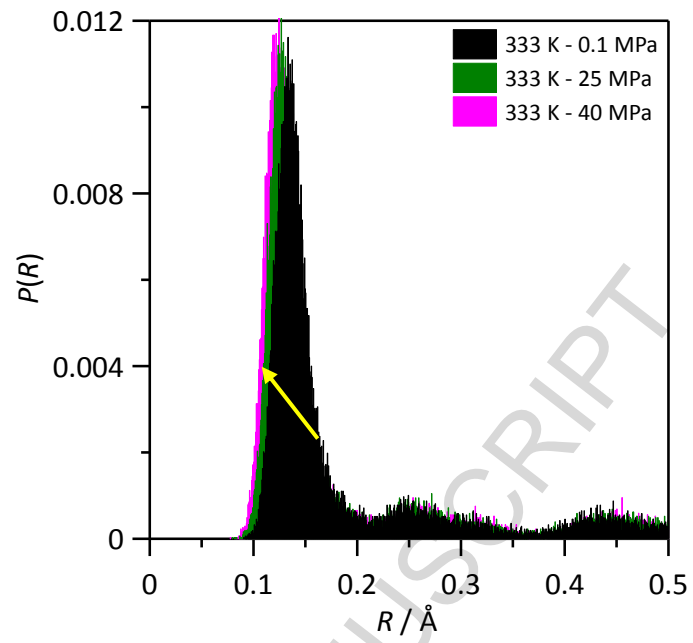
Figure 12

Figure 13

40
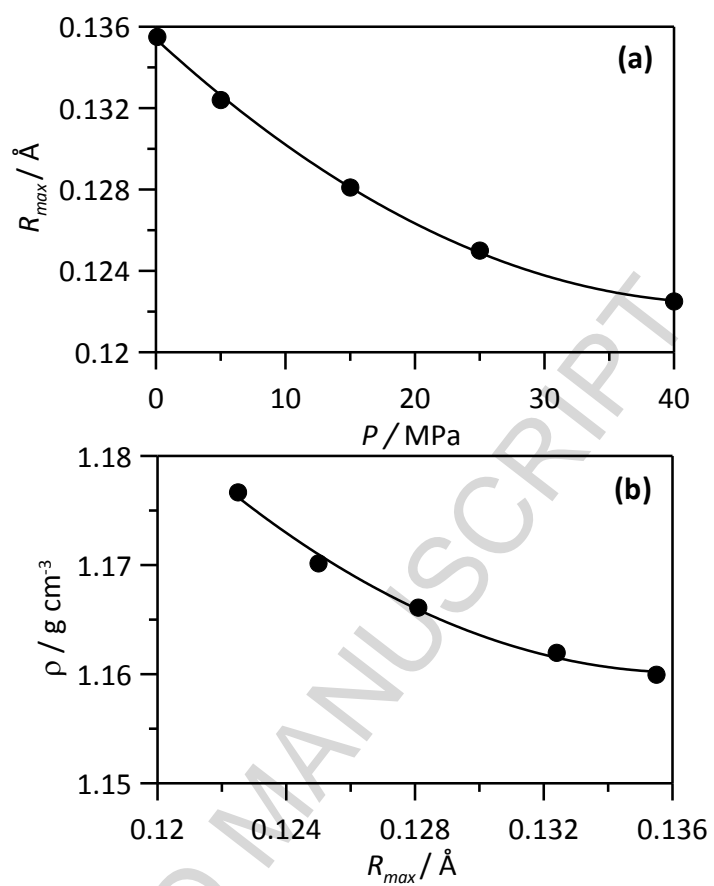
Highlights

- Protic ionic liquids.
- High pressure.
- PVT behavior.
- Molecular dynamics.
- Hydrogen bonding.